

# Resolving the bow-shock nebula around the old pulsar PSR B1929+10 with multi-epoch Chandra observations

C. Y. Hui and W. Becker

Max-Planck Institut für Extraterrestrische Physik, Giessenbachstrasse 1, 85741 Garching bei München, Germany

the date of receipt and acceptance should be inserted later

**Abstract.** We have studied the nearby old pulsar PSR B1929+10 and its surrounding medium utilizing the sub-arcsecond angular resolution of Chandra. The Chandra data are found to be fully consistent with the results obtained from deep XMM-Newton observations as far as the pulsar is concerned. The non-thermal emission nature of the pulsar's X-radiation is confirmed. In addition to the X-ray trail seen already in previous observations by ROSAT and XMM-Newton an arc-like nebula intimately surrounding the pulsar is discovered at a signal-to-noise ratio of  $\sim 5$ . Using two Chandra observations separated by about six months morphological variability of this arc-like nebula is indicated.

**Key words.** pulsars: individual PSR B1929+10—stars: neutron—X-rays: stars

## 1. Introduction

In the 90's of the last century a series of powerful X-ray observatories were launched to space. Among many great results on various aspects in astrophysics they allowed a first detailed study of the X-ray emission properties of rotation-powered pulsars as a class (cf. Becker & Trümper 1997; Becker & Pavlov 2001 for a review). Most old<sup>1</sup> radio pulsars, though, were still too faint for a detailed study by these satellites (cf. Sun et al. 1993; Manning & Willmore 1994; Becker & Trümper 1997; Saito 1998). Old pulsars are clearly in the domain of the XMM-Newton and Chandra observatories. Observations of PSR B0950+08, B0823+26, J2043+2740 (Becker et al. 2004; Zavlin & Pavlov 2004), B0628-28 (Becker et al. 2005), B0943+10 (Zhang, Sanwal & Pavlov 2005), B1133+16 (Kargaltsev, Pavlov & Garmire 2006), B1929+10 (Becker et al. 2006) and B2224+65 (Hui & Becker 2007) have finally allowed a first detailed view to the emission properties of old pulsars as a class. Surprisingly, the X-ray emission from old pulsars seems to be largely dominated by non-thermal radiation processes. Thermal components (e.g. account for the emission from hot polar caps) are not required to model the X-ray spectra of these pulsars. Further support for an emission scenario dominated by non-thermal radiation is found by the observed temporal emission properties. Pulse profiles, if detected with sufficient photon statistics, show multiple components and narrow features. This is indicative of strongly

beamed emission which further invalidates the heated polar cap scenario as the main source of X-ray emission in old pulsars. The pulsed fractions in old pulsars are in the range of  $\sim 30 - 50\%$ .

In addition to the pulsar emission which is originating within the co-rotating magnetosphere extended trail-like X-ray emission was observed from PSR B1929+10 (Becker et al. 2006) and PSR B2224+65 (Hui & Becker 2007) on a scale of several arc-minutes. In the case of PSR B1929+10 the X-ray emission in the trail is interpreted as synchrotron emission produced in the shock between the pulsar wind and the surrounding medium (see the discussion in Becker et al. 2006 for details). Owing to the moderate ( $15''$  Half Energy Width) spatial resolution of XMM-Newton, details of the nebular emission associated with PSR B1929+10 might have been remained unresolved. With a ten times improved angular resolution Chandra data can thus be essential to further constrain the properties of the nebula very near to the pulsar.

In this paper we present a detailed analysis of multi-epoch Chandra observations of the field around PSR B1929+10<sup>2</sup>. According to its X-ray emission properties this source can be considered to be prototypical of an old pulsar (Becker et al. 2006). With a pulse period of  $P = 226.5$  ms and a period derivative of  $\dot{P} = 1.16 \times 10^{-15}$ , its characteristic age is determined to be  $\sim 3 \times 10^6$  years. These spin parameters imply a spin-down luminosity of  $\dot{E} = 3.9 \times 10^{33}$  erg s<sup>-1</sup> and a magnetic field at the neutron star magnetic poles of  $B_{\perp} \sim 5 \times 10^{11}$  G. With a radio dispersion measure of  $3.178$  pc cm<sup>-3</sup>, the NE2001 Galactic free electron density model of Cordes & Lazio (2002) predicts a distance of 170 pc. However, the recent astromet-

<sup>1</sup> In standards of high energy astronomy rotation-powered pulsars are called young, middle aged and old if their spin-down age is of the order of few times  $10^3 - 10^4$  yrs,  $10^5 - 10^6$  yrs and  $\geq 10^6$  yrs, respectively. This classification is diffuse, though, with a smooth transition in between the different groups.

<sup>2</sup> A brief X-ray study of PSR B1929+10 with Chandra was recently presented by Misanovic, Pavlov & Garmire (2006).

**Table 1.** Ephemerides of PSR B1929+10 <sup>a</sup>

Right Ascension (J2000)	19 <sup>h</sup> 32 <sup>m</sup> 13.983 <sup>s</sup> ± 0.002 <sup>s</sup>
Declination (J2000)	+10° 59′ 32.41″ ± 0.07″
First date for valid parameters (MJD)	52929
Last date for valid parameters (MJD)	53159
Pulsar rotation period (s)	0.2265182954
Period derivative $\dot{P}$ ( $10^{-15}$ s s <sup>-1</sup> )	1.164739
Characteristic age ( $10^6$ yrs)	3.09
Surface dipole magnetic field ( $10^{12}$ G)	0.5129
Dispersion Measure (pc cm <sup>-3</sup> )	3.178
Distance (pc)	361 <sup>+10</sup> <sub>-8</sub>
Spin-down Luminosity ( $10^{33}$ ergs s <sup>-1</sup> )	3.89

<sup>a</sup>Adopted from Becker et al. (2006)

ric measurements by Chatterjee et al. (2004) yielded a precise proper motion and parallax determination that translates into an accurate distance measurement of  $d = 361^{+10}_{-8}$  pc and a proper motion of  $V_{\perp} = 177^{+4}_{-5}$  km s<sup>-1</sup>. The ephemerides of PSR B1929+10 which we made use of in this paper are listed in Table 1.

The paper is organized as follows: in §2 we describe the observations and data analysis, in §3 we summarize the results and provide a discussion relative to the results obtained by XMM-Newton.

## 2. Observations and data analysis

Data analysis is restricted to the energy range 0.5–8.0 keV. All energy fluxes, however, are computed for the 0.5–10 keV band for better comparison with the results based on XMM-Newton data (Becker et al. 2006).

PSR B1929+10 was observed with Chandra in 2005 December 04 (Obs ID: 6657) and 2006 May 28 (Obs ID: 7230) with the Advanced CCD Imaging Spectrometer (ACIS). In both observations, PSR B1929+10 was located on the back-illuminated (BI) ACIS-S3 chip with an off-axis angle of  $\sim 0.1$  arcmin. Standard processed level-2 data were used. The effective exposures are  $\sim 21$  ks and  $\sim 25$  ks for the observations in 2005 December and 2006 May, respectively.

### 2.1. Spatial analysis

The X-ray images of the  $5 \times 5$  arcmin field centered on PSR B1929+10 as well as a close-up of the central  $1 \times 1$  arcmin regions are shown in Figure 1 for both epoches. A compact nebula which has an arc-like morphology resembling somewhat a bow-shock is clearly detected intimately around PSR B1929+10 in both observations. The signal-to-noise ratios of this compact features are  $\sim 5.6$  and  $\sim 5.0$  in the 2005 December and 2006 May observation, respectively. We estimate that due to the wings of the point spread function (PSF)  $\sim 50\%$  to the total counts in the nebula can be from the pulsar. The contribution from the PSF wings, though, is symmetric for

these on-axis observations and thus cannot result in the asymmetric shape as observed.

Comparing the fields from both epochs, we noticed that there are indications for variations in the morphology of this nebula features. The compact structures, however, are at the detection threshold which prevents us from any final conclusions on it but rather calls for independent confirmation in deeper observations. In addition to the features near to the pulsar a clumpy structure (which is labeled as C in Figure 1b) is observed in the December 2005 data. There are only  $\sim 24$  net counts from this clump which does not allow a more detailed analysis on it. The signal-to-noise ratio of this clump is estimated to be  $\sim 2$  and thus is still in agreement with being background fluctuation. In the 2006 May data the signal-to-noise ratio of the emission in this region is even smaller.

In Figures 1a and 1c no prominent structure resembling the X-ray trail seen by ROSAT and XMM-Newton opposite to the pulsar’s proper motion direction can be identified (cf. Figure 2 in Becker et al. 2006). We have further examined the Chandra images by smoothing the raw data with a kernel of  $\sigma < 6$  arcsec which is comparable with the FWHM of XMM-Newton’s PSF. The smoothed images are displayed in Figure 2. Comparing the images with the contours calculated from XMM-Newton MOS1/2 data, a faint trail-like feature is noticed. However, the background contribution of this feature is estimated to be  $\sim 60\%$ . The unabsorbed X-ray flux of a 1 arcmin circular trail region near to the pulsar as detected by XMM-Newton is  $f_{\chi} = 5.3 \times 10^{-14}$  erg/s/cm<sup>2</sup> within the 0.5–10 keV band (Becker et al. 2006). The low significance of the trail in the two Chandra observations thus is in agreement with Chandra’s lower sensitivity. We therefore will not further consider the X-ray trail emission in this paper and forward the interested reader to Becker et al. (2006) for a detailed discussion of its emission properties.

### 2.2. Spectral analysis

Although the spectrum from PSR B1929+10 has already been constrained tightly using XMM-Newton data (Becker et al. 2006) it is still essential for us to re-examine its spectral properties with Chandra since it better resolves the pulsar emission from the compact surrounding nebular component.

We extracted the pulsar spectrum in both data sets from a circle of 2 arcsec radius (encircled energy  $\sim 95\%$ ), centered on the pulsar, and fitted both simultaneously. The background spectrum was extracted from a source free region within a 10 arcsec radius centered at R.A.=19<sup>h</sup>32<sup>m</sup>13.982<sup>s</sup>, Dec.=10°59′47.63″ (J2000). After background subtraction, 595 and 678 net counts were available for the spectral analysis, implying a net counting rate of  $(2.85 \pm 0.12) \times 10^{-2}$  cts/s and  $(2.75 \pm 0.11) \times 10^{-2}$  in both data sets.

Response files were computed by using the CIAO tools MKRMF and MKARF. The pulsar spectra were dynamically binned so as to have at least 30 counts per bin. To better constrain the spectral properties, we fitted the spectra obtain from both observations simultaneously. All the spectral fittings were performed in 0.5–8 keV by using XSPEC 11.3.2. The degrada-

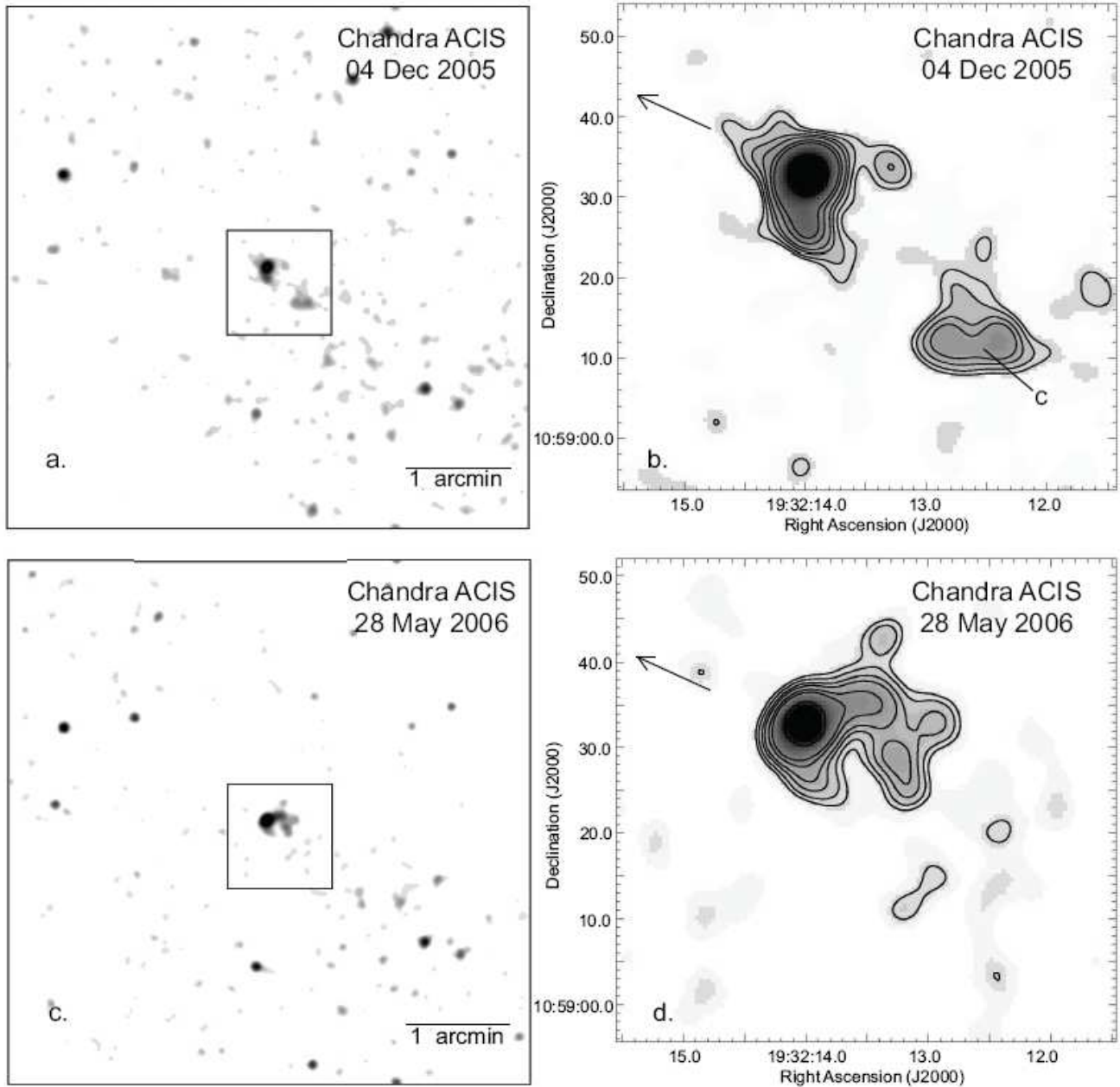


**Fig. 1.** (a)  $5 \times 5$  arcmin view centered on PSR B1929+10 as observed by Chandra in the energy band of 0.5 – 8 keV on 04 Dec 2005. Top is north and left is east. The image is binned with a factor of 0.5 arcsec and adaptively smoothed with a kernel of  $\sigma < 2$  arcsec. (b) The close-up view of the central  $1 \times 1$  arcmin region as illustrated in a. PSR B1929+10 is the brightest source in the field. An arc-like feature associated with the pulsar is observed. The proper motion direction of the pulsar is illustrated by the arrow. (c) Similar as a but for the observation on 28 May 2006. (d) Similar as b but for the observation on 28 May 2006. All images are produced with the same intensity-color mapping for better comparison. Contour lines at the levels of  $(6.4\text{--}58.0) \times 10^{-6}$  counts arcsec $^{-2}$  s $^{-1}$  are overlaid in Fig. 1b and d.

tion of the ACIS quantum efficiency for each observations was corrected individually by using the XSPEC model ACISABS. The parameters of all fitted model spectra are summarized in Table 2. All the quoted errors are  $1 - \sigma$  and were computed for 1 parameter of interest.

Among the single component models which were tested we found that a power-law model fits the data best ( $\chi^2_\nu = 0.83$

for 36 D.O.F.). This model yields a column density of  $N_H = 1.13^{+0.33}_{-0.37} \times 10^{21}$  cm $^{-2}$ , a photon index of  $\Gamma = 2.82^{+0.15}_{-0.14}$  and a normalization at 1 keV of  $8.29^{+0.99}_{-0.98} \times 10^{-5}$  photons keV $^{-1}$  cm $^{-2}$  s $^{-1}$ . These best-fit values are very well consistent with those obtained by XMM-Newton (see Table 3 in Becker et al. 2006). The best-fit power-law spectrum and residuals are shown in Figure 3. We have also computed the error contours

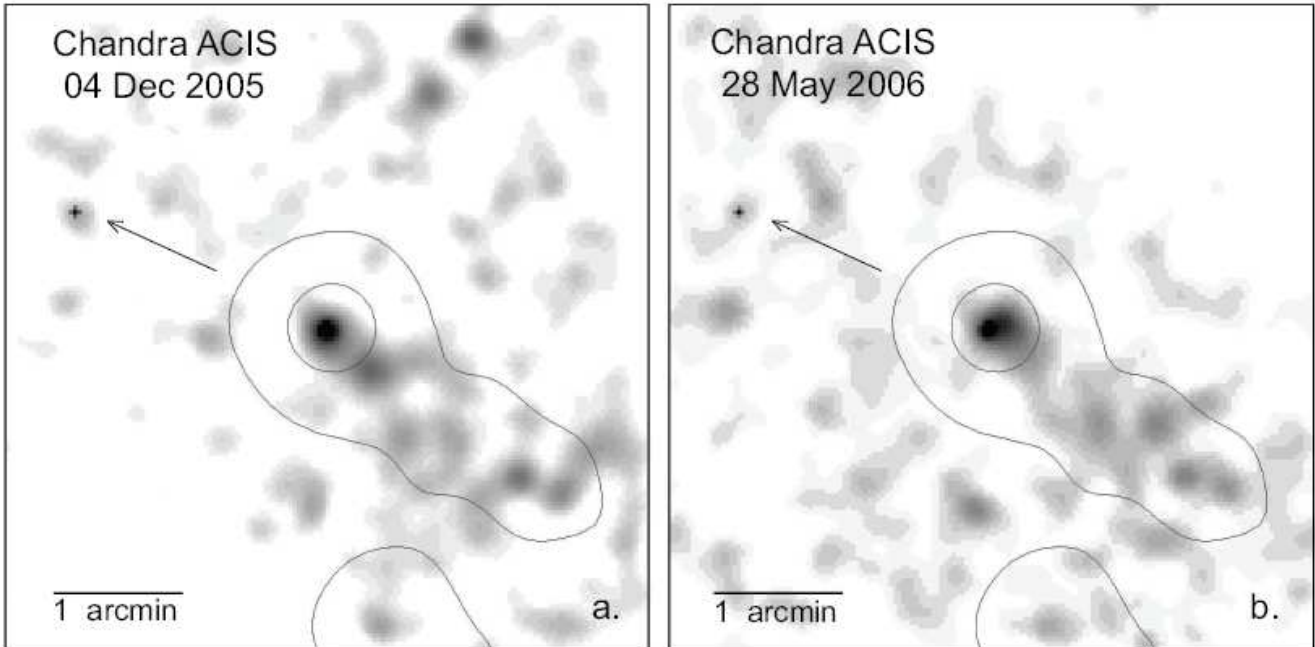


**Fig. 2.** (a)  $5 \times 5$  arcmin region around PSR B1929+10 observed by Chandra in the energy band of 0.5 – 8 keV on 04 Dec 2005. The image is produced with a binning factor of 2 arcsec and adaptively smoothed with a kernel of  $\sigma < 6$  arcsec. Top is north and left is east. (b) Similar as a but for the observation on 28 May 2006. The contours calculated at the level of 0.09 and 0.44 counts arcsec $^{-2}$  from the XMM-Newton’s MOS1/2 image in the energy band 0.2 – 10 keV are overlaid on both images to illustrate the correspondence. The proper motion direction of the pulsar is illustrated by the arrow in the images.

to demonstrate the relative parameter dependences of the photon index vs. the hydrogen column density and plotted this in Figure 4. The unabsorbed flux deduced for the best fit power-law model parameters is  $f_X = 2.6 \times 10^{-13}$  ergs s $^{-1}$  cm $^{-2}$  within 0.5 – 10 keV. At a distance of 361 pc it implies a luminosity of  $L_X = 4.1 \times 10^{30}$  ergs s $^{-1}$ .

As for the XMM-Newton data it is obvious that the single power-law model already describes the observed pulsar spectrum very well. Hence, the justification of including an additional thermal component is absent. In the Chandra data, we found that fitting with a power-law plus blackbody model does not yield a stable solution if one let both blackbody radius and temperature be free parameters. Fixing the blackbody radius at the size of a classic polar cap (i.e.  $r_{pc} = R(2\pi R/cP)^{1/2} \sim 300$  m) does result in a stable fit which yields  $T \sim 9.4 \times 10^5$  K. For the blackbody radius fixed at the canonical size of the neutron star, e.g. 10 km, we obtain  $T \sim 5.6 \times 10^5$  K. We quantify the statistical significance for adding an extra component to the power-law model with the  $F$ -test which suggest that inclusion of such thermal components is only required at a confidence level  $\lesssim 65\%$ . Due to the better photon-statistics this number was even smaller in the XMM-Newton data (Becker et al. 2006). This low significance is also reflected by the relative contribution of the thermal component in the total energy flux observed by Chandra. For any thermal polar-cap contribution  $\sim 13\%$  is the  $1\sigma$  limit.

For the spectral model consisting of two blackbody components, we found that the best-fitted model parameters also agree well with those inferred from the XMM-Newton spec-

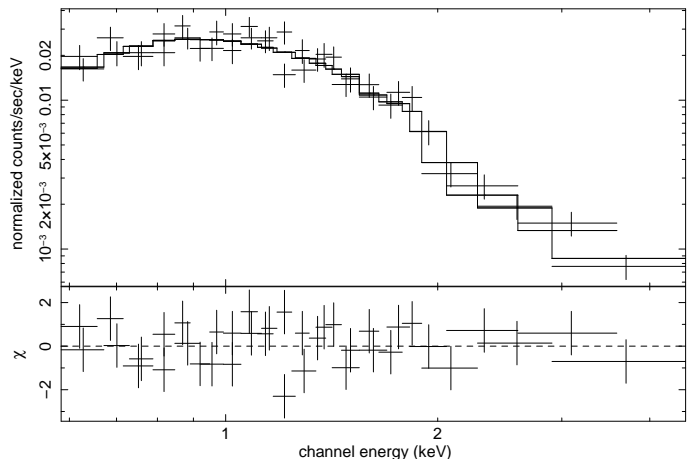


**Fig. 3.** Energy spectra of PSR B1929+10 as observed with the Chandra ACIS-S3 detector on 04 Dec 2005 and 28 May 2006 and simultaneously fitted to an absorbed power-law model (*upper panel*) and contribution to the  $\chi^2$  fit statistic (*lower panel*).

tra (Becker et al. 2006). Despite the acceptable value of the goodness-of-fit, the pulsar spectrum obtained by XMM-Newton has already shown that such model cannot describe the data beyond  $\sim 5$  keV (see Becker et al. 2006).

Since the arc-like feature is resolved by Chandra for the first time, it is instructive to examine its energy spectrum, albeit the photon statistics is small. Since morphological variability of the feature is indicated (see Figure 2), we extracted the spectra of

**Table 2.** Spectral parameters inferred from fitting the Chandra observed spectra of PSR B1929+10 and the associated extended feature.

Model <sup>a</sup>	$\chi^2_\nu$	D.O.F.	$N_H$ $10^{21} \text{ cm}^{-2}$	$\Gamma^b / kT$	Normalization at 1 keV <sup>c</sup> photons $\text{keV}^{-1} \text{ cm}^{-2} \text{ s}^{-1}$	Radius <sup>d</sup> m
PSR B1929+10						
PL	0.83	36	$1.13^{+0.33}_{-0.37}$	$2.82^{+0.15}_{-0.14}$	$8.29^{+0.99}_{-0.98} \times 10^{-5}$	-
BB	2.95	36	0.00	0.31	-	43.32
PL+BB	0.85	35	$1.12^{+0.59}_{-0.36}$	$2.80^{+0.19}_{-0.15}/0.08^{+0.03}_{-0.08}$	$8.25^{+1.25}_{-2.24} \times 10^{-5}$	300
PL+BB	0.84	35	$1.48^{+1.10}_{-0.59}$	$2.89^{+0.27}_{-0.18}/0.05^{+0.01}_{-0.05}$	$8.92^{+2.37}_{-1.22} \times 10^{-5}$	10000
BB+BB	0.89	34	< 0.4	$0.56^{+0.07}_{-0.05}/0.20^{+0.02}_{-0.02}$	-	$10.80^{+2.46}_{-2.60}/95.53^{+30.59}_{-15.85}$
Arc-like feature						
PL	0.52	7	< 1.30	$1.31^{+0.35}_{-0.30}$	$2.58^{+0.87}_{-0.57} \times 10^{-6}$	-

<sup>a</sup> PL = power-law; BB = blackbody

<sup>b</sup> The entry in this column depends on the model in interest. It is the temperature  $kT$  in keV or the photon index  $\Gamma$

<sup>c</sup> The normalization constant for the power-law model.

<sup>d</sup> The radius of the blackbody emitting area is calculate for a assumed pulsar distance of 361 pc.

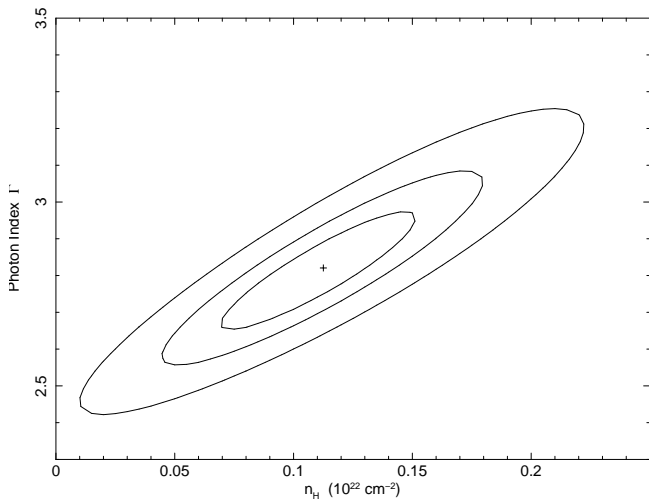


**Fig. 4.**  $1\sigma$ ,  $2\sigma$  and  $3\sigma$  confidence contours calculated for 1 parameter of interest for the power-law model fitted to the spectrum of PSR B1929+10.

the feature from the regions in accordance with the morphology in the corresponding observations.

In the 2005 Dec observation, we covered the whole arc-like structure with 2 circular regions with the radii 2.7 and 3 arcsec located at R.A.=19<sup>h</sup>32<sup>m</sup>13.249<sup>s</sup>, Dec.=+10°59′33.16″ (J2000) and R.A.=19<sup>h</sup>32<sup>m</sup>13.708<sup>s</sup>, Dec.=+10°59′22.21″ (J2000), respectively, as well as an annular region centered on the pulsar position with inner and outer radii of 2″ and 8″ so as to minimize the contribution from the pulsar. The background spectrum is extracted from a nearby source free region within a circle of 10″ radius centered at R.A.=19<sup>h</sup>32<sup>m</sup>12.245<sup>s</sup> and

Dec.=+10°59′35.94″ (J2000). After background subtraction, there are 33 net counts extracted from the arc-like feature.

In the 2006 May observation, the spectrum of the extended feature was extracted from an annular region centered on the pulsar position with the inner and outer radii 2″ and 5″, a  $5 \times 6$  arcsec box centered at R.A.=19<sup>h</sup>32<sup>m</sup>13.805<sup>s</sup>, Dec.=+10°59′25.56″ (J2000) and oriented 25° east from the north and a  $18 \times 8$  arcsec box centered at R.A.=19<sup>h</sup>32<sup>m</sup>13.293<sup>s</sup>, Dec.=+10°59′31.90″ (J2000) oriented 25° east from the north.

The background spectrum was extracted from a nearby source free region within a circle of 10 arcsec radius centered at RA.=19<sup>h</sup>32<sup>m</sup>14.314<sup>s</sup> and Dec.=+10°59′48.73″ (J2000). After background subtraction, there are 48 net counts extracted from the arc-like feature.

The spectra from both data sets did not show any evidence for temporal spectral variability. We hence have fitted both spectra simultaneously. We binned the data dynamically so as to have at least 10 counts per spectral bin. We found that a power-law model can provide a reasonable description of the feature’s spectrum ( $\chi_\nu = 0.52$  for 7 D.O.F.). The best-fit power-law spectrum and residuals are shown in Figure 5. This model yields a column density of  $N_H < 1.30 \times 10^{21} \text{ cm}^{-2}$ , a photon index of  $\Gamma = 1.31^{+0.35}_{-0.30}$  and a normalization at 1 keV of  $2.58^{+0.87}_{-0.57} \times 10^{-6} \text{ photons keV}^{-1} \text{ cm}^{-2} \text{ s}^{-1}$ . We constrained the relationship between the photon index and the column density by calculating the error contours at various confidence levels. The contour plot is shown in Figure 6. After correcting the contribution from the PSF wing centered at the pulsar, the unabsorbed flux deduced for the best-fitted model parameters are  $f_X = 1.3 \times 10^{-14} \text{ erg s}^{-1} \text{ cm}^{-2}$  in the energy range of 0.5 – 10

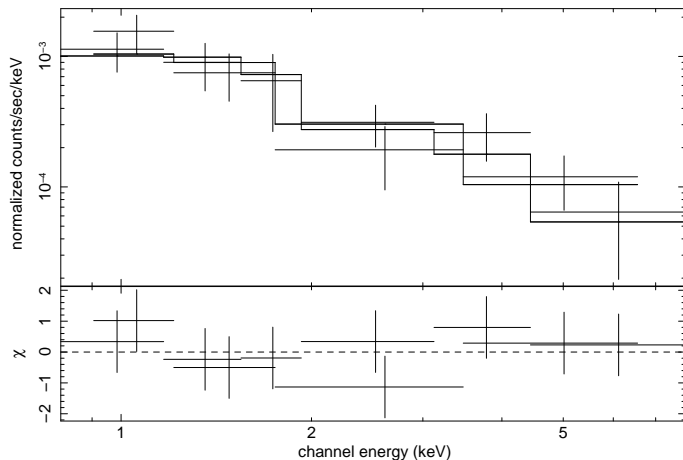


**Fig. 5.** Energy spectra of the arc-like structure associated with PSR B1929+10 as observed by the Chandra ACIS-S3 detector on 04 Dec 2005 and 28 May 2006 and simultaneously fitted to an absorbed power-law model (*upper panel*) and contribution to the  $\chi^2$  fit statistic (*lower panel*).

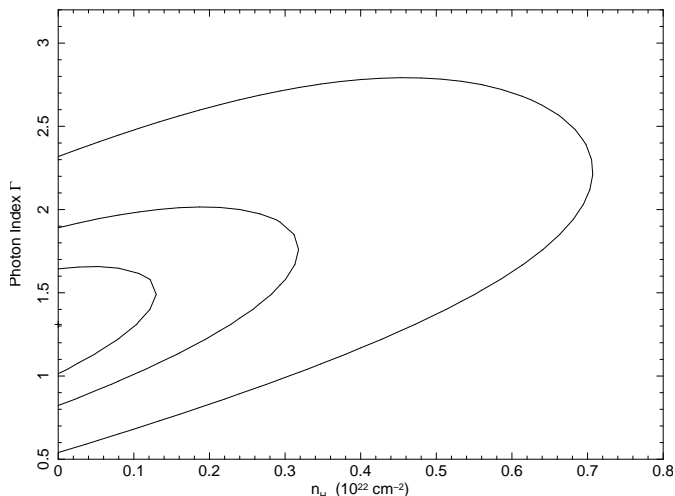


**Fig. 6.**  $1\sigma$ ,  $2\sigma$  and  $3\sigma$  confidence contours calculated for 1 parameter of interest for the power-law model fitted to the spectrum of the arc-like nebula associated with PSR B1929+10.

keV. The pulsar distance of 361 pc implies a luminosity of  $L_X = 2.0 \times 10^{29}$  erg s $^{-1}$ .

We have checked the robustness of the spectral results by incorporating background spectra extracted from different source-free regions. We found that within the  $1\sigma$  errors the spectral parameters inferred from independent fittings are all consistent with each other.

### 3. Discussion

Complementing the XMM-Newton observation, we have studied PSR B1929+10 and its surrounding medium with Chandra which provides us data with sub-arcsecond resolution. So far three distinct components have been resolved, namely the pulsar itself, the X-ray trail opposite to the pulsars proper motion direction as well as the arc-like nebula intimately surrounding the pulsar. The flux contributions from these components

**Table 3.** Unabsorbed fluxes, luminosities and the conversion efficiencies of PSR B1929+10 and the nebular components in 0.5 – 10 keV

Component	$f_X$ ergs s $^{-1}$ cm $^{-2}$	$L_X^a$ ergs s $^{-1}$	$L_X/E$
PSR B1929+10	$2.6 \times 10^{-13}$	$4.1 \times 10^{30}$	$1.0 \times 10^{-3}$
Trail-like feature <sup>b</sup>	$5.3 \times 10^{-14}$	$8.3 \times 10^{29}$	$2.1 \times 10^{-4}$
Arc-like feature	$1.3 \times 10^{-14}$	$2.0 \times 10^{29}$	$5.1 \times 10^{-5}$

<sup>a</sup> Luminosities are calculated at the assumed pulsar distance of 361 pc

<sup>b</sup> Adopted from Becker et al. (2006)

and the corresponding X-ray conversion efficiencies are summarized in Table 3.

For PSR B1929+10, we found that the spectral properties inferred from our analysis are in excellent agreement with the results obtained by XMM-Newton which did not allow the pulsar emission to be separated from the compact nebular component. The consistency is not unexpected even in the presence of the diffuse compact nebulae which contributes only  $\sim 5\%$  to the observed energy flux (see Table 3). Thus, the non-thermal emission scenario of PSR B1929+10 is confirmed. Hui & Becker (2007) had argued that it is possible to sustain particle acceleration regions in PSR B1929+10’s outer-magnetosphere (so-called outer-gap) if the inclination of the magnetic axis with respect to the rotational axis is taken into account. This inference is supported by the ability of the outer-gap model in reproducing the observed X-ray pulse profile and its phase shift relative to the radio pulse (see Fig. 16 Becker et al. 2006). However, such model is not without difficulty in explaining the observed properties of PSR B1929+10.

In the outer-gap model, the non-thermal X-rays result from the back-flowing charge particles from the outer gap (Cheng & Zhang 1999). When the primary electrons/positrons leave the outer-gap, they will emit curvature photons which are subsequently converted into secondary pairs in the presence of the strong magnetic field. Synchrotron photons will then be emitted by these secondary electrons/positrons. If these photons are energetic enough, they will further be converted into pairs which again lose their energy via synchrotron radiation. Therefore, an electromagnetic cascade is developed. Based on this model, Cheng & Zhang (1999) argued that the X-ray photon index resulting from such cascades should be  $\leq 2$ . This is obviously not in agreement with the observed photon index for PSR B1929+10 which is as steep as  $2.82^{+0.15}_{-0.14}$ . Observations of five other old pulsars: B1133+16 (Kargaltsev, Pavlov & Garmire 2006), B0943+10 (Zhang, Sanwal & Pavlov 2005), B0628-28 (Becker et al. 2005), B0823+26 (Becker et al. 2004) and J2043+2740 (Becker et al. 2004), also found the photon indices steeper than 2. This gives the outer-gap emission model a challenge. Re-examination of the model is thus required.

For the arc-like nebula, its morphology and the orientation with respect to the pulsar’s proper motion direction sug-

gest a bow-shock nature. It is noticed to be asymmetric in the Chandra data (see Fig. 1 b & d). Such asymmetric X-ray nebula was firstly observed in the field around PSR J2124-3358 (Hui & Becker 2006). As argued in Becker et al. (2006), PSR B1929+10 is likely to be moving supersonically in the ISM and the shape of the bow-shock nebula is determined by the balance between the wind particles and the surrounding ISM. Hence, its asymmetric shape might be a result of the anisotropic pulsar wind and/or inhomogeneities in the surrounding ISM. Comparing two frames with an epoch separation of  $\sim 6$  months, morphological variability of the arc-like nebula is suggested. The nebular extent was found to vary by  $\sim 0.2$  arcmin. At the pulsar distance of 361 pc, the change of extent is  $\sim 0.02$  pc. This requires the variability to take place at a speed of  $\sim 0.1c$ , where  $c$  is the speed of light. Hence, such morphological change is physically feasible. If this can be confirmed, it will be an exciting example to witness the time-varying interaction between the pulsar wind and the ISM. Nevertheless, the limited photons collected from the nebula does not allow any final conclusion to be drawn. Moreover, there are many stars located in the field around PSR B1929+10 (cf. Fig. 6 in Becker et al. 2006) which may also contribute to the variable emission. In view of these ambiguities, deeper Chandra observations are essential in constraining the physical properties of this interesting nebula with higher significance. Optical observations are also required to discriminate whether the morphological variability is indeed caused by the pulsar-ISM interaction or as a result of the varying field stars.

*Acknowledgements.* We thank Bernd Aschenbach for thoroughly reading the manuscript and provide us with many useful comments.

## References

- Becker, W., Jessner, A., Kramer, M., Testa, V., & Howaldt, C. 2005, *ApJ*, 633, 367
- Becker, W., & Pavlov, G. G. 2001, in *The Century of Space Science*, eds. J. Bleeker, J. Geiss & M. Huber, Kluwer Academic Publishers, p721 (available from astro-ph/0208356).
- Becker, W., & Trümper, J. 1997, *A&A*, 326, 682
- Becker, W., Weisskopf, M. C., Tennant, A. F., Jessner, A., Dyks, J., Harding, A. K., & Zhang, S. N. 2004, *ApJ*, 615, 908
- Becker, W., Kramer, M., Jessner, A., et al. 2006, *ApJ*, 645, 1421
- Chatterjee, S., Cordes, J. M., Vlemmings, W. H. T., Arzoumanian, Z., Goss, W. M., & Lazio, T. J. W. 2004, *ApJ*, 575, 407
- Cheng, K. S., & Zhang, L. 1999, *ApJ*, 515, 337
- Cordes, J. M., & Lazio, T. J. W. 2002, preprint (astro-ph/0207156)
- Hui, C. Y., & Becker, W. 2006, *A&A*, 448, L13
- Hui, C. Y., & Becker, W. 2007, *A&A*, 467, 1209
- Kargaltsev, O., Pavlov, G. G., & Garmire, G. P. 2006, *ApJ*, 636, 406
- Manning, R. A., & Willmore, A. P. 1994, *MNRAS*, 266, 635
- Misanovic, Z., Pavlov, G. G., & Garmire, G. P. 2006, AAS HEAD meeting 9
- Saito, Y. 1997, Ph.D. thesis, Univ. Tokyo
- Sun, X., Trümper, J., Dennerl, K., & Becker, W. 1993, *IAU Circ.*, 5895, 2
- Zavlin, V. E., & Pavlov, G. G. 2004, *ApJ*, 616, 452
- Zhang, B., Sanwal, D., & Pavlov, G. G. 2005, 624, L109